



Experimental study on seismic response of soilbags-built retaining wall

Si-Hong Liu^{a,b}, Fan Jia^{b,*}, Xiao-Lin Chen^c, Ling-Jun Li^c

^a State Key Laboratory of Hydrology-Water Resources and Hydraulic Engineering, Hohai University, Nanjing, 210098, China

^b College of Water Conservancy and Hydropower Engineering, Hohai University, Xi-Kang Road 1#, Nanjing, 210098, China

^c China Design Group Co. Ltd, Zi-Yun Road 9#, Nanjing, 210014, China



ARTICLE INFO

Keywords:

Geosynthetics
Soilbags
Retaining wall
Seismic performance
Shaking table test

ABSTRACT

The seismic performance of soilbags-built retaining wall model was studied experimentally. A series of small-scale shaking table tests with the input of different amplitude sinusoidal waves and a large-scale shaking table test in a designed laminar shear box with the input of the Wenchuan earthquake wave were carried out on soilbags' retaining wall models. For comparison, the small-scale shaking table tests were also conducted on horizontally reinforced retaining wall models. The horizontal acceleration responses, the Fourier spectra, the dynamic earth pressure and the lateral displacements of soilbags' retaining wall models were investigated in shaking table tests. The results show that the seismic response of the soilbags' retaining wall is equivalent to or even slightly better than that of the horizontally reinforced retaining wall. The fundamental frequency and the Fourier spectral characteristics of the soilbags' retaining wall are similar to those of backfill sands. The dynamic earth pressure of the wall model fluctuates almost synchronously with the input Wenchuan wave and no residual earth pressure is induced by the seismic loading. The permanent lateral displacements are small when subjected to multiple shakings, providing a proof that the retaining wall of soilbags has a good seismic performance.

1. Introduction

Earth retaining walls are commonly used in water conservancy, civil engineering, transportation and other fields. They are usually classified into two major types according to their deformation characteristics: rigid retaining walls and flexible retaining walls. The former ones are mainly made of concrete or masonry, and the latter ones are commonly referred to reinforced retaining walls, in which planar geosynthetic sheets (e.g. geotextiles and geogrids) or steel strips are commonly embedded horizontally within retaining walls (Rowe and Skinner, 2001; Sukmak et al., 2016; Yazdandoust, 2017a) and subgrades (Giroud and Han, 2004; Chen et al., 2015). The engineering practices show that flexible retaining walls, especially geosynthetic-reinforced soil (GRS) walls have more satisfactory seismic performances than rigid ones. Collin et al. (1992) reported that Geo-synthetic Reinforced Soil (GRS) walls survived the Loma Prieta earthquake of 1989 with estimated ground accelerations ranging from 0.3 to 0.7 g. Many conventional gravity type retaining walls as well as numerous cantilever-type reinforced concrete retaining walls were seriously damaged during the 1995 Hyogoken-Nanbu earthquake in Japan (Koseki et al., 1998), whereas geosynthetic reinforced-soil (GRS) retaining walls performed well (Tatsuoka et al., 1996). The similar phenomena were also observed after the 2008 Wenchuan earthquake (Zhang et al., 2012). Matsuoka

and Liu (2003) proposed an earth-reinforcement method with soilbags, i.e., wrapping soils in entirely closed geotextile containers. As a result of extensive studies on soilbags (Matsuoka et al., 2000a, 2000b; Matsuoka and Liu, 1999, 2003), Matsuoka and Liu (2006) suggested that soilbags could be used to construct retaining walls, which might also be regarded as a new type of GRS retaining wall.

Many researches have been conducted on GRS retaining walls, especially on their seismic performance. These studies have applied various methodologies including full-scale structures (e.g. Bathurst et al., 2009; Koseki, 2012; Yang et al., 2012; Riccio et al., 2014; Liu et al., 2019), reduced-scale models (e.g. El-Emam and Bathurst, 2007; Nakajima, 2008; Sabermahani et al., 2009; Huang et al., 2011; Ehrlich et al., 2012; Ling et al., 2012; Liu et al., 2017; Yazdandoust, 2018; Huang, 2019; Ren et al., 2020; Li et al., 2020), numerical analysis (e.g. Skinner and Rowe, 2005; Liu et al., 2014a; Yu et al., 2017; Fan et al., 2020) and laboratory tests on reinforced soil (Tavakoli Mehrjardi et al., 2012; Moghaddas Tafreshi et al., 2014; Plácido et al., 2018). Bathurst et al. (2005) established a working stress method for the calculation of reinforcement loads in GRS walls using a database of instrumented and monitored full-scale field and laboratory walls. Shaking table tests facilitate testing of the seismic performance of GRS walls. Futaki et al. (1996) studied the natural frequency and dynamic response of GRS walls with different wall heights through large-scale shaking table tests.

* Corresponding author.

E-mail addresses: sihongliu@hhu.edu.cn (S.-H. Liu), kv@hhu.edu.cn (F. Jia), cxlndyx@126.com (X.-L. Chen), 798478638@qq.com (L.-J. Li).

El-Emam and Bathurst (2004, 2007) provided the experimental design, equipment and instrumentation for a reinforced soil wall response using shaking table tests and carried out reduced-scale model shaking table tests with rigid facing panels to investigate the reinforcement design parameters.

Compared to GRS walls, fewer studies have been conducted on the retaining wall of soilbags. A small number of studies are mainly focused on the static performance of soilbags retaining wall (Fan et al., 2019; Wang et al., 2019c) and the dynamic properties of stacked soilbags (Cheng et al., 2016, 2017; Wang et al., 2019b). Liu et al. (2014c, 2016) investigated the distribution of the earth pressures behind a soilbags-stacked retaining wall and the lateral transmission in the retaining wall through laboratory experiments. The results demonstrate that the stability of soilbags-constructed retaining walls is closely related to the interlayer friction of soilbags depending on the bag friction, the grain sizes of filling materials and the interlayer arrangements of soilbags. In the soilbags-constructed retaining wall, soilbags are subjected to external loads not parallel to the short axis of soilbag. Liu et al. (2018) theoretically investigated the strength characteristics of soilbags under inclined loads and numerically simulated them using DEM. The dynamic properties of stacked soilbags were studied through a series of cyclic lateral shear tests (Liu et al., 2014b). The test results illustrate that soilbags have a relatively high damping ratio and variable horizontal stiffness, which are significantly influenced by the infill materials at a low vertical stress but become nearly independent of the infill materials at a high vertical stress. A primary design method for soilbags-constructed retaining walls has been proposed by Liu (2017). Several application cases and the well performance of this new type wall have been reported (Matsuoka and Liu, 2006; Wang et al., 2015a, 2019a; Liu et al., 2015, 2019). The studies and applications show that the soilbags-constructed retaining wall has the advantages of weight light and good adaptation to foundation deformation like GRS retaining wall.

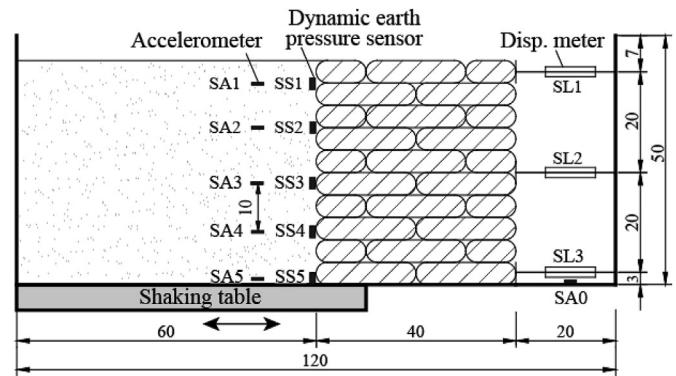
This paper presents the investigation of the seismic response of the soilbags-stacked retaining wall model through shaking table tests. Firstly, the seismic performance of the soilbags' retaining wall was qualitatively investigated through a series of small-scale shaking table tests with the input of a sinusoidal wave and different accelerations. Then, a large-scale shaking table test was conducted in a designed laminar shear box with the input of a seismic wave recorded during the Wenchuan earthquake.

2. Small-scale shaking table tests

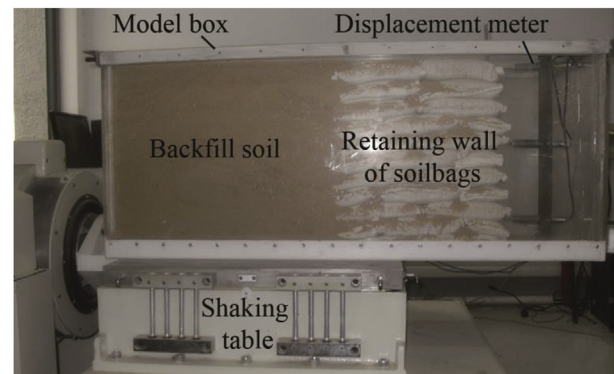
The most advantage of the small-scale shaking table is of its easy and quick performance. To qualitatively understand the seismic response of soilbags' retaining wall and horizontal reinforced retaining wall, a series of small-scale shaking table tests were conducted under different dynamic base shaking with the input of a sinusoidal wave, focusing on the seismic lateral displacements, dynamic earth pressures and horizontal acceleration response. Since it is a comparative test and has no actual project background, the similitude laws are ignored in the tests.

2.1. Test setup

Fig. 1 shows the setup of the small-scale shaking table test on soilbags-stacked wall. The small-scale shaking table was electromagnetically controlled. It has a surface size of 70 cm × 70 cm, a maximum gravity capacity of 300 kg, a maximum acceleration of 490 m/s², and an operating frequency of 5–2000 Hz. A plexiglass-made rectangle model box with a size of 120 cm × 50 cm × 45 cm was bolted on the surface of the shaking table. A piece of sandpaper was placed at the bottom of the model box to prevent the sliding between the retaining wall and the bottom plate. The vertical inner surface of the model box was coated with silicone grease and covered with a layer



(a)



(b)

Fig. 1. Schematic diagram and photograph of the small-scale shaking table test (unit: cm): (a) schematic diagram; (b) photograph.

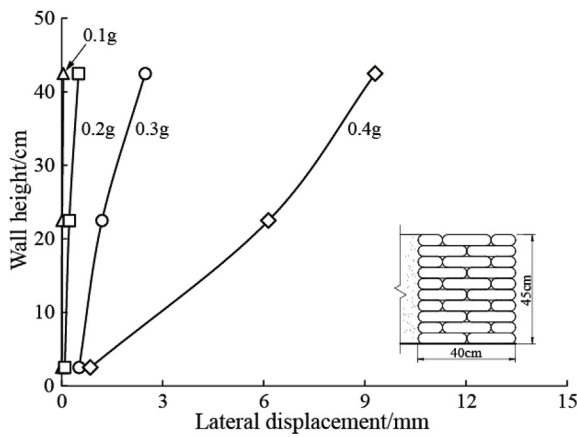
of plastic film to reduce the friction between the retaining wall and the model box.

The retaining wall model was 40 cm wide by 45 cm high, staggered with ten layers of soilbags (two sizes: 20 cm × 20 cm × 4.5 cm and 20 cm × 10 cm × 4.5 cm). The soilbags were made by filling river sand into woven bags, which were made of polypropylene (PP) and had the weight of 84 g per-square meter, the elongation more than 25%, the warp and weft tensile strength of 7.7 kN/m and 5.7 kN/m, respectively. The river sand has the maximum grain size of 5 mm, the non-uniform coefficient C_u of 2.04 and the curvature coefficient C_c of 1.08. The internal friction angle and cohesion of the river sand are 35.4° and 3.25 kPa, respectively. The same river sand was backfilled behind the retaining wall, which was placed into the model box in five layers and compacted to be a density of 1.75 g/cm³.

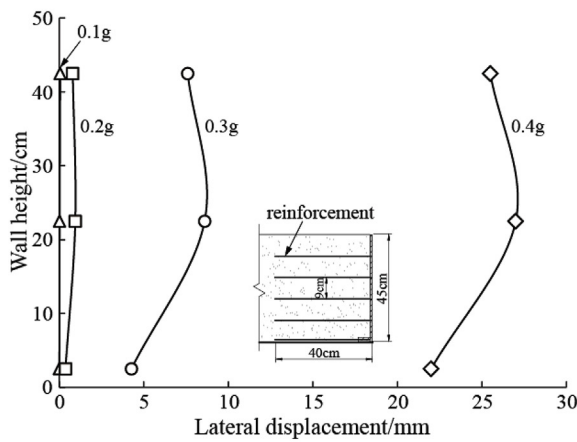
Five horizontal accelerometers (SA1-SA5) were installed in the backfill sand along the height and one horizontal accelerometer (SA0) was placed on the surface of the shaking table. Three displacement meters (SL1-SL3) were installed onto one batten that was fixed by one steel frame to measure the lateral displacements of the wall. Five strain pressure sensors (SS1-SS5) were installed behind the wall along the height to measure the dynamic earth pressures.

For comparison, the shaking table tests were also performed on a retaining wall that was horizontally reinforced with 5 layers of geotextile strips. The geotextile strip has the same width as the soilbags wall. It has a unit weight of 160 g/m², the elongation more than 25% and the warp and weft tensile strength 25.8 kN/m and 16.2 kN/m, respectively.

The tests were carried out under five different input peak accelerations of 0.1 g, 0.2 g, 0.3 g and 0.4 g with the same sine waves and the frequency of 6 Hz. The shaking lasted 50s in each test.



(a)



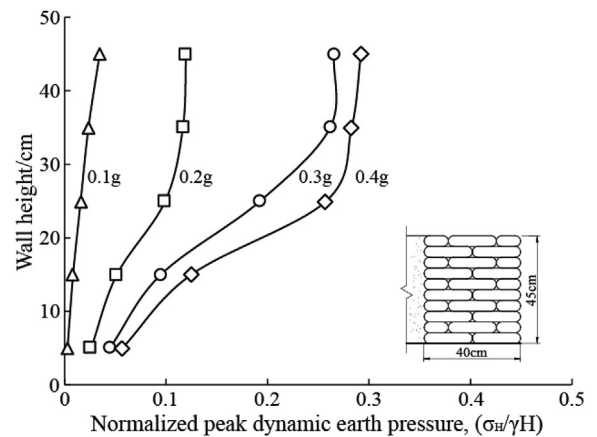
(b)

Fig. 2. Lateral displacements along the wall height at different input accelerations ($f = 6$ Hz): (a) soilbags-stacked wall; (b) horizontally reinforced soil wall.

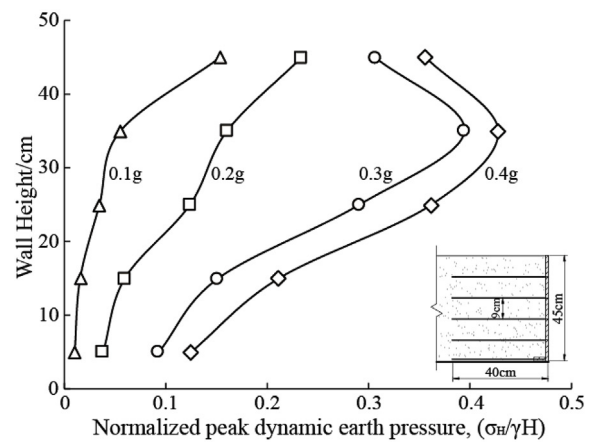
2.2. Test results

Fig. 2 shows the distribution of the lateral displacements of the retaining wall model along the wall height at different input base accelerations. It can be seen that the lateral displacements of the retaining wall of soilbags are large at the top and small at the bottom, similar to the horizontal shaking of a cantilever beam, while the maximum lateral displacements of the horizontally reinforced soil wall take place nearly in the middle height of the wall. When the input acceleration is less than 0.2 g, the lateral displacements of the two retaining walls are less than 1 mm; when the input acceleration is larger than 0.3 g, the lateral displacements of the two walls begin to increase significantly. Overall, the lateral displacement of the soilbags-stacked wall is less than that of the horizontally reinforced soil wall, especially at the lower part of the wall. At the input acceleration of 0.4 g, the maximum lateral displacements of the soilbags-stacked wall and the horizontally reinforced soil wall are 9 mm and 27 mm, respectively.

Determining the actual change in lateral earth pressure is one of the most important factors in the optimal design of reinforced soil structures (Yazdandoust, 2017b; Wang et al., 2018). To compare the dynamic earth pressure of the two different kinds of retaining walls, the measured peak dynamic earth pressures (σ_H) were normalized to the soil unit weight (γ) and the wall height (H). Fig. 3 shows the



(a)



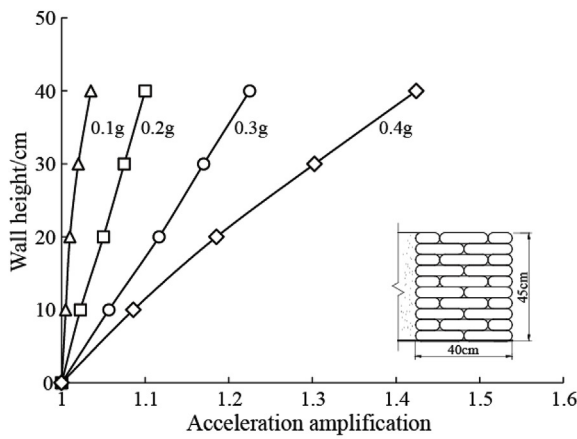
(b)

Fig. 3. Dynamic earth pressure coefficients along the wall height under different input accelerations: (a) soilbags-stacked wall; (b) horizontally reinforced soil wall.

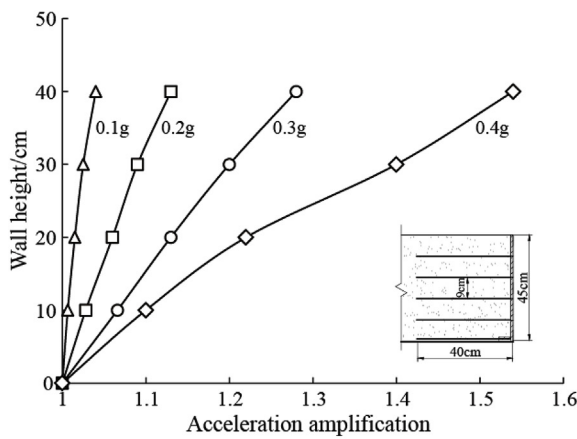
distributions of normalized dynamic earth pressures along the wall height at different input base accelerations. Similar distributions along the wall height have been observed, but the magnitudes of the soilbags-stacked wall are smaller at the same height. It demonstrates that at the input base accelerations of 0.1 g and 0.2 g, the normalized dynamic earth pressures of the two retaining walls have nearly linear increasing tendency with the wall height, while they depict different curved shapes at the input base accelerations of 0.3 g and 0.4 g. At the input base acceleration of 0.4 g, the maximum normalized dynamic earth pressures of the reinforced soil wall and the soilbags-stacked wall are 0.43 and 0.29, respectively.

Fig. 4 shows the amplification of input base accelerations of the two retaining walls along the wall height, in which the amplification factor is the ratio of the acceleration measured within the backfill sand to the input base acceleration. It demonstrates that the amplification factors almost linearly increase along the wall height in the two kinds of the wall models regardless of what input base accelerations. However, the magnitudes in the soilbags-stacked wall are slightly smaller than those in the horizontally reinforced soil wall under the same conditions.

The above test results demonstrate qualitatively that the seismic response of the soilbags-stacked retaining wall is equivalent to or even slightly better than that of the horizontally reinforced soil wall.



(a)



(b)

Fig. 4. Amplification of input base acceleration along the wall height ($f = 6$ Hz): (a) soilbags-stacked wall; (b) horizontally reinforced soil wall.

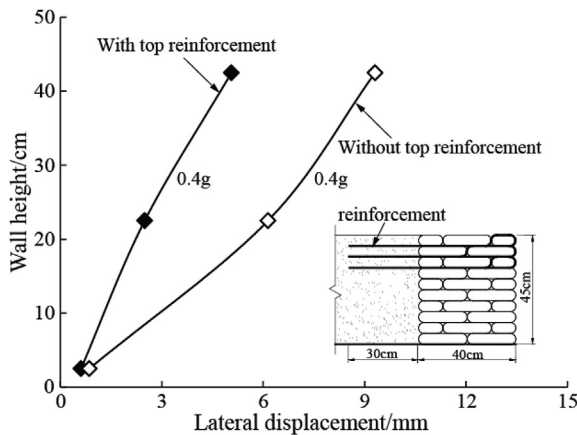


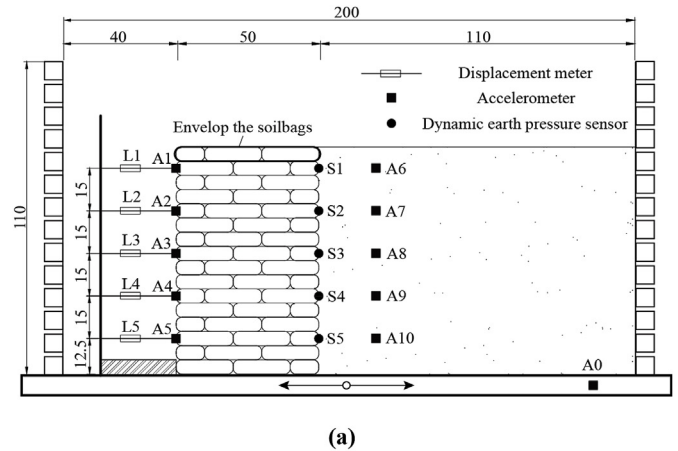
Fig. 5. Comparison of the lateral displacements of the wall with and without the top reinforcement.

2.3. Improvement of the soilbags-stacked retaining wall

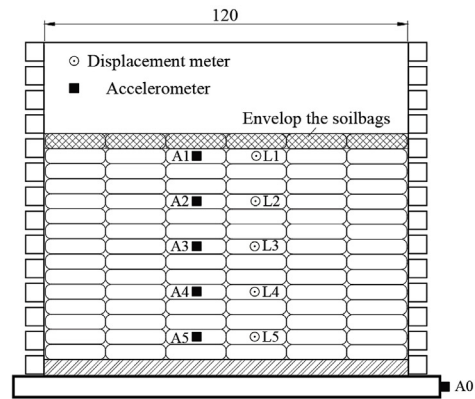
As shown in Fig. 2(a), the maximum lateral displacements of the soilbags-stacked retaining wall happen at the top under different input base accelerations, indicating that the soilbags at the top of the retaining wall are prone to fall during the horizontal shaking. To prevent

Table 1
Scaling factors for the shaking table model.

Variable	Parameter	Similitude rule	Scaling factor
Length	l	S_l	6
Density	ρ	S_ρ	1
Acceleration	a	S_a	1
Velocity	v	$S_v = S_l^{1/2}$	2.45
Displacement	u	$S_u = S_l$	6
Cohesion	c	$S_c = S_a S_\rho S_l$	6
Frictional angle	ϕ	$S_\phi = 1$	1
Time	t	$S_t = S_l^{1/2} S_a^{-1/2}$	2.45
Frequency	ω	$S_\omega = S_l^{-1/2} S_a^{1/2}$	0.41
Force	F	$S_F = S_a S_\rho S_l^3$	216



(a)



(b)

Fig. 6. General arrangement and instrument layout of retaining wall model of soilbags (Unit: cm): (a) cross section; (b) front view.

the fall of the top soilbags and increase the stability of the retaining wall, the top three-layers of soilbags were enveloped with geotextile strips, as shown in the insert of Fig. 5. The outermost soilbag in each of the top three layers was wrapped with the extended end of the geotextile strip placed on the lower layer of soilbags. The geotextile strips are the same as used in horizontally reinforced soil wall. Fig. 5 shows the comparison of the lateral displacements of the wall with and without the top reinforcement under the shaking of 0.4 g base acceleration. The comparison illustrates that the reinforcement of the top three layers can reduce significantly the lateral displacement of the wall, which provides an effective way to improve the seismic performance of the retaining wall of soilbags.

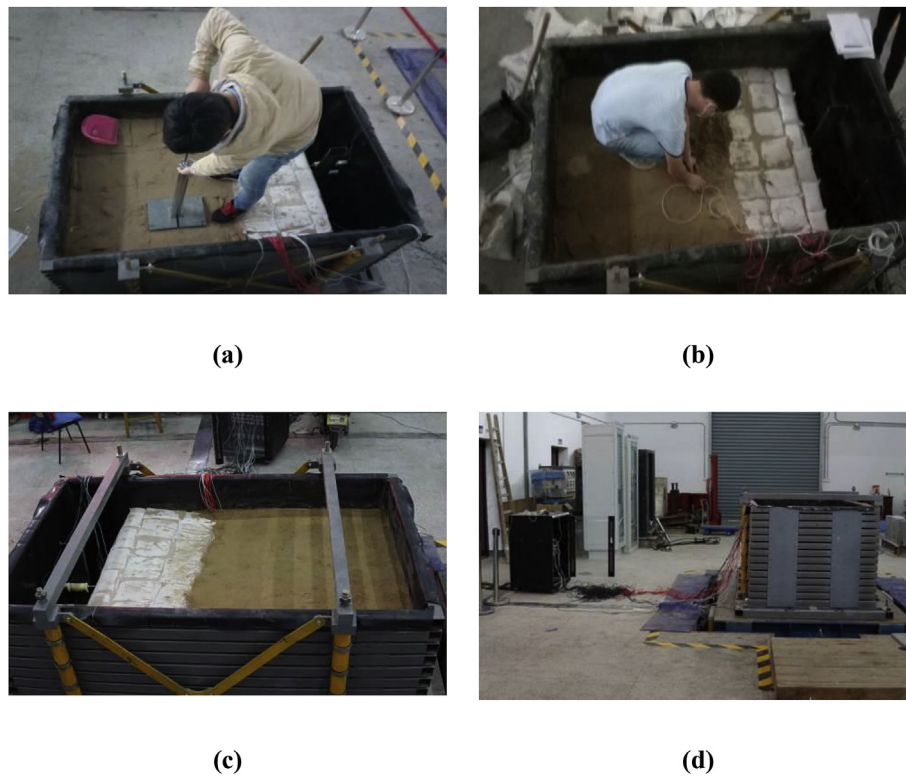


Fig. 7. Preparation for retaining wall model of soilbags and instruments installation.

3. Large-scale shaking table test

3.1. Test equipment

The tests were carried out on a 2.0 m × 2.8 m shaking table that was served by an electro-hydraulic energy control system. The shaking table has the maximum horizontal acceleration of ± 1.2 g, the operating frequency of 0.1–100 Hz and the maximum gravity capacity of 6×10^3 kg. The soilbags' retaining wall model was constructed in a laminar shear container of 2.0 m (Length) × 1.2 m (Width) × 1.1 m (Height), which composed of 14-layer laminated frames. Each frame was made of four steel tubes with a square cross-section of 60 mm × 60 mm and the thickness of 3 mm, and frictionless ball bearings were placed between laminated frames. The laminar shear container has two advantages over the conventional rigid model boxes (Chen et al., 2010): 1) the vibration of the soil near the wall of the laminar shear container is hardly restricted, so that the seismic wave can propagate outward at the interface of the laminated frames with less scattered and reflected waves produced; 2) it can simultaneously deform with the backfill soil.

3.2. Similitude rule

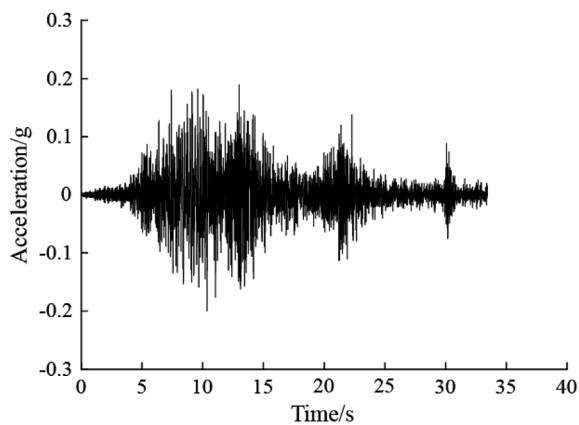
To study the seismic response characteristics of the retaining wall and the backfill sand, the similitude rules of the various physical and mechanical variables were exported by the Buckingham's π theorem in dimensional analysis theories. In this study, basic physical variables needed in the similitude rule were chosen to be length, density and acceleration. In view of the ability of shaking table facility, an 80 cm-high model of soilbags-stacked retaining wall was designed with the 1/6 scaling factor (S), equivalent to a 4.8 m height prototype. Meanwhile, the values of scaling ratio for the density and the acceleration were both fixed at 1.0 to make the prototype soil applicable in shaking table tests. Subsequently, the scaling ratios for some main parameters of the experimental model can be deduced by taking the length, the density and

the acceleration as control variables based on the Buckingham π theorem, as listed in Table 1.

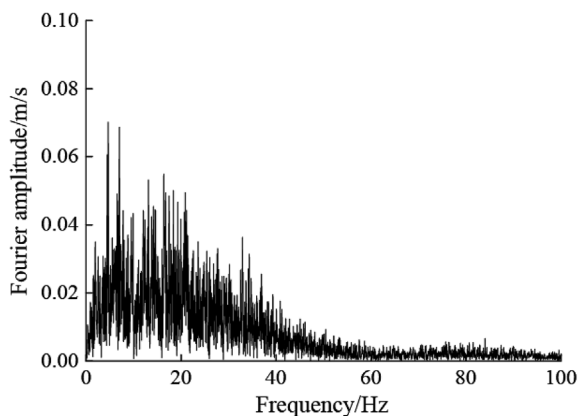
3.3. Test setup and instrument layout

In the laminar shear container, a retaining wall model of soilbags with dimensions of 120 cm wide by 50 cm thick by 80 cm high was constructed with 16 layers of soilbags, which were vertically arranged in a staggered form. Behind the retaining wall, river sands were back-filled in the container with a length of 110 cm. The soilbags and the river sands are the same as those used in the small-scale shaking table tests. The soilbags at the top layer of the retaining wall were enveloped with a geogrid. Fig. 6 shows the general arrangement and the instrument layout of the retaining wall model of soilbags. Ten horizontal accelerometers were installed in the testing model, five onto the wall surface (A1–A5) and five inside the backfill sand (A6–A10). One horizontal accelerometer was set on the shaking table platform to record the acceleration response of the shaking table. Five dynamic displacement meters (L1–L5) were installed onto a fixed steel frame to measure the lateral displacements of the wall. Five dynamic earth pressure sensors (S1–S5) were installed behind the wall to record the dynamic earth pressure response of the retaining wall during the shaking test.

Fig. 7 shows the preparation for the retaining wall model of soilbags and instruments installation in the laminar shear container. In the test model, the moisture content and the density of the backfill sand were controlled to be 3% and 1.66 g/cm^3 , respectively. Each layer of soilbags was slightly compacted and leveled with a small platen hamper. The backfill sands were simultaneously placed with the soilbags. After the placement of each two layers of soilbags, the backfill sands were compacted to the desired density of 1.66 g/cm^3 (Fig. 7(a)). The monitoring instruments were embedded in the pre-set position during the construction of the soilbags' wall model, as shown in Fig. 7(b). After completing the model, the laminar shear container was lifted and moved onto the shaking table by a crane, and then bolted on the shaking table. Finally, all the instruments were connected to a data



(a)



(b)

Fig. 8. Time-history and Fourier spectrum of compressed Wenchuan wave (time scaling factor: 2.45): (a) input wave; (b) Fourier spectrum.

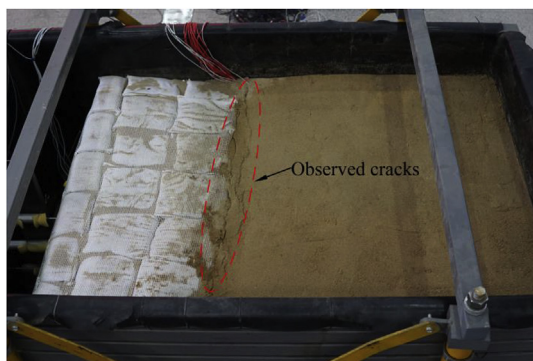


Fig. 9. Observed crack at the interface between the wall and the backfill sands after the shaking test.

acquisition system, as shown in Fig. 7(c) and (d).

3.4. Test conditions

In this study, the horizontal seismic wave measured during the Wenchuan earthquake in China in 2008 (Wenchuan wave) was used as the external excitation of the wall model, as shown in Fig. 8. The model was subjected to several different excitations from weak (low amplitude) to strong (high amplitude) peak base accelerations, as shown in

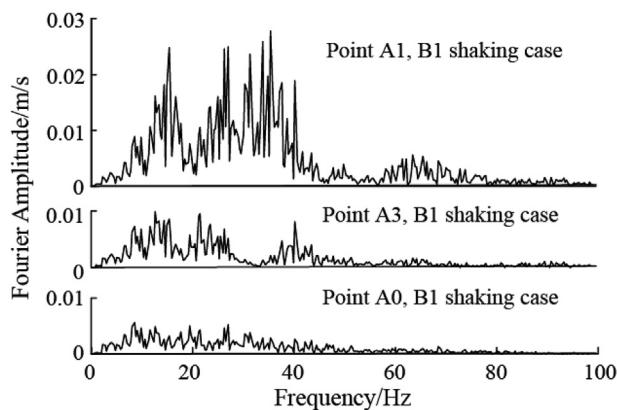


Fig. 10. Fourier spectra of the horizontal acceleration response for test points A1, A3 and A0 under B1 shaking case.

Table 1. To acquire the fundamental frequency of the testing retaining wall model, a 30 s white noise wave was added before each shaking under the Wenchuan wave, which is a random noise signal with bandwidth of 1–100 Hz and root mean square (RMS) acceleration of 0.05 g.

3.5. Test results and discussion

3.5.1. Observed phenomenon

During the shaking tests under different input peak accelerations, the seismic response of the retaining wall and the surface of the backfill sands were closely observed. The retaining wall model of soilbags was slightly shaken and basically intact under shaking cases of W1-0.1 g and W2-0.2 g. When the input peak acceleration increased to 0.4 g, small cracks happened at the interface between the wall and the backfill sands. Under the shaking case of W4-0.6 g, the retaining wall shook violently, and the crack developed across the whole surface of the backfill sands after the shaking test, as shown in Fig. 9.

3.5.2. Spectral characteristics of the wall model under white noise wave

As aforementioned, a 30 s white noise wave was added before the first shaking under the Wenchuan wave. Fig. 10 shows the Fourier spectra for the test points in front of the wall model and on the shaking table under B1 case. It is seen that the Fourier amplitude of the input white noise wave (point A0) changes slightly within 0–50 Hz. However, the Fourier amplitudes of the test points in front of the wall are quite different from the point A0, which increase along the wall height. For the test point A1 at the top of the wall, there are two peaks around 15 Hz and 33 Hz, corresponding to two fundamental frequencies. These different spectral characteristics along the wall height will cause different dynamic responses under the seismic wave.

Furthermore, a white noise wave was also added after each shaking test under the Wenchuan wave with different peak accelerations. Fig. 11 shows the Fourier spectra for the test point A1 at the top of the wall under the cases of B2, B3, B4 and B5. It is found that the magnitudes and the positions of the peak Fourier amplitudes are different under the four shaking cases, illustrating that the fundamental frequencies of the wall model change after the shaking under the Wenchuan wave with different peak accelerations.

3.5.3. Acceleration response of wall under Wenchuan wave

Fig. 12 shows the time history of the horizontal acceleration response and Fourier spectra for test points A1 and A3 in front of the wall under the shaking case of W4-0.6 g. It demonstrates that the peak accelerations of the wall model increase along the wall height from the bottom to the top, with the values of 0.72 g, and 1.17 g at test points A3, and A1, respectively. This increasing trend was also observed in

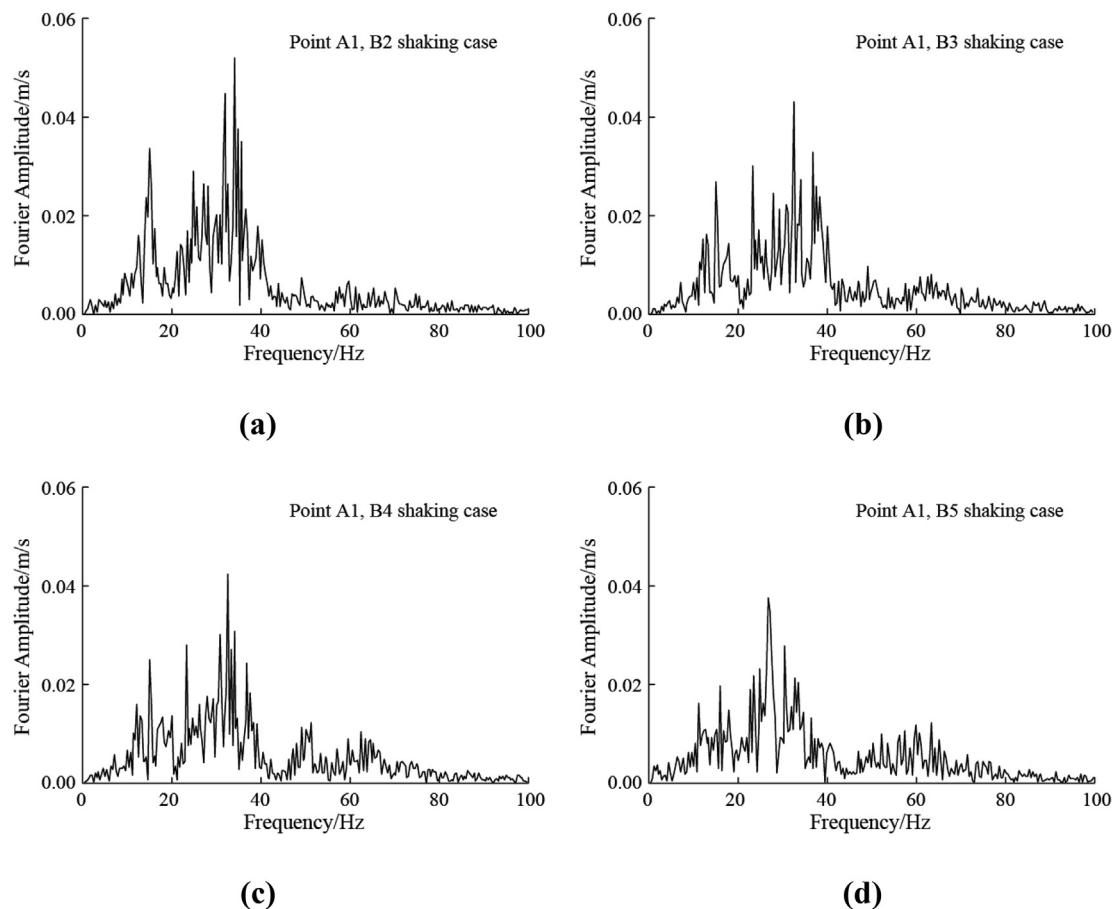


Fig. 11. Fourier spectra of the horizontal acceleration response for the test point A1 under B2, B3, B4 and B5 shaking cases: (a) B2; (b) B3; (c) B4; (d) B5.

rigid retaining walls and reinforced earth retaining walls (Lin et al., 2017; Yazdandoust, 2017a; Wang et al., 2015b). The Fourier spectra results illustrate that the peak accelerations of the wall model are within the frequency less than 40 Hz. Compared to the input Wenchuan wave (Fig. 8(b)), the Fourier amplitude of the wall model increases at the frequency of 5–15 Hz, while the Fourier amplitude is filtered out at the frequency larger than 20 Hz.

Fig. 13 presents the Fourier spectra of backfill sands at test points A6 and A8 under the shaking case of W4-0.6 g. The peak Fourier amplitudes appear within the frequency range of 5–15 Hz, similar to those of test points A1 and A3 at the same height (see Fig. 12). The similarity of the Fourier spectra of backfill sands with the wall at the same height means that their fundamental frequencies are nearly the same. That is to say, the stiffness of soilbags' retaining wall is close to that of backfill sands, so that the retaining wall can deform basically together with the backfill sands.

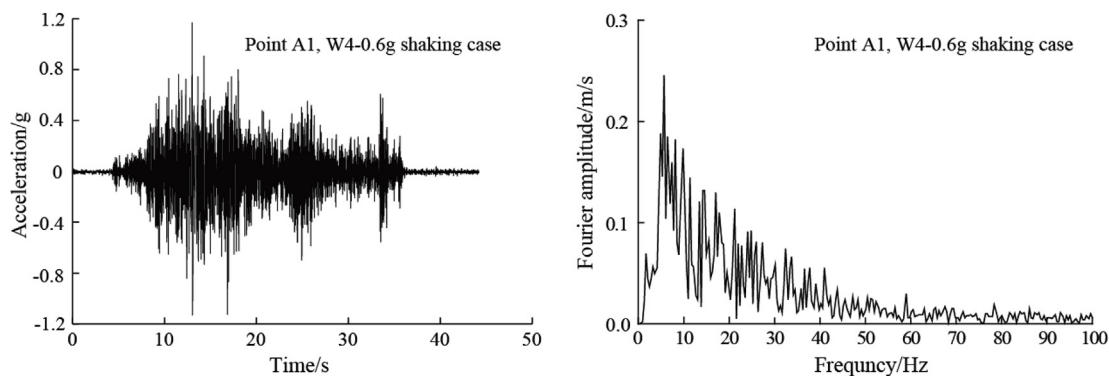
Fig. 14 gives the Fourier spectra for test point A1 under the shaking cases of W1-0.1 g, W2-0.2 g and W3-0.4 g. It demonstrates that at the input peak acceleration of 0.1 g, the Fourier spectrum of the retaining wall of soilbags has two peaks (i.e. the amplification effects) in the frequency ranges of 5–15 Hz and 25–35 Hz, respectively. With the increasing input peak acceleration, the Fourier amplitude increases within the 5–15 Hz and decreases within the 25–35 Hz. At the input peak acceleration of 0.6 g, only one peak appears within the frequency range of 5–15 Hz (see Fig. 12(a)). This means that the fundamental frequency of the retaining wall of soilbags decreases with the increasing input peak acceleration. As listed in Table 2, the retaining wall model of soilbags was subjected to a series of shakings under the Wenchuan wave with increasing peak acceleration. After each shaking, the stiffness of the retaining wall model of soilbags might decrease slightly. It is

considered that the shaking numbers also contribute to the decrease of the fundamental frequency in Fig. 14.

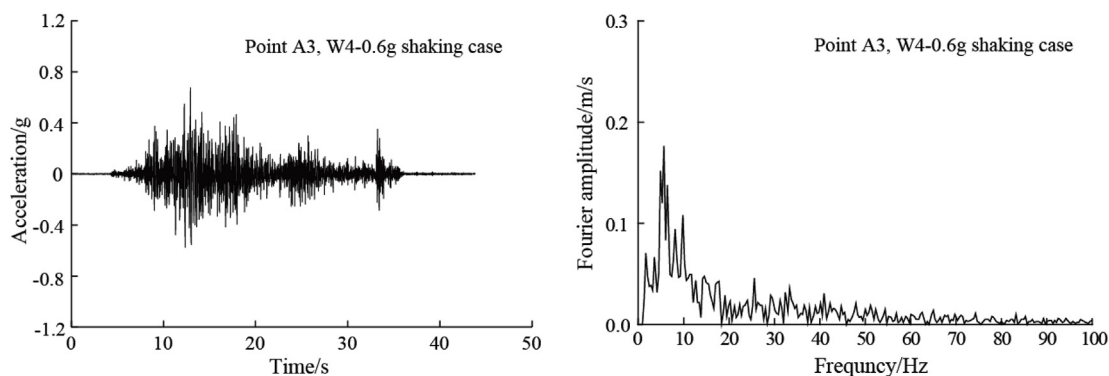
The horizontal peak acceleration amplification, which is defined as the ratio of the horizontal peak acceleration response measured at test points to that on the shaking table platform in time history, is adopted to evaluate the effect of the horizontal acceleration amplification. Fig. 15 shows the distributions of the horizontal peak acceleration amplification along the wall height under the four shaking cases of W1-0.1 g to W4-0.6 g. It is seen that the acceleration amplification increases along the wall height, and a dramatic increase exists at the height of 60 cm, representing the whipping effect of the flexible structure. At the same wall height, the acceleration amplification tends to decrease when the input peak acceleration increases from 0.1 g to 0.4 g, and turns to increase when the input peak acceleration increases from 0.4 g to 0.6 g. This is because no interlayer slipping of soilbags occurs in the retaining wall when the input peak acceleration is small (less than 0.4 g). In these cases, the decrease of the acceleration amplification may result from the increase of the friction energy dissipation due to the frictional motion of sand particles in bags during the shaking. However, when the input peak acceleration reaches 0.6 g, the retaining wall shakes violently, leading to the interlayer slipping of soilbags and the increase of the acceleration amplification of the retaining wall.

3.5.4. Dynamic earth pressure response

The dynamic earth pressure on the retaining wall of soilbags under the shaking case of W4-0.6 g is typically studied. The initial earth pressure induced by self-weight is removed to only analyze the dynamic earth pressure increment under seismic loading. Fig. 16 shows the time history of dynamic earth pressure at test point S5, in which the positive value refers to a compressive pressure. It is found that the dynamic



(a)



(b)

Fig. 12. Acceleration time histories and Fourier spectra for test points A1 and A3 in front of the wall under W4-0.6 g shaking case: (a) A1; (b) A3.

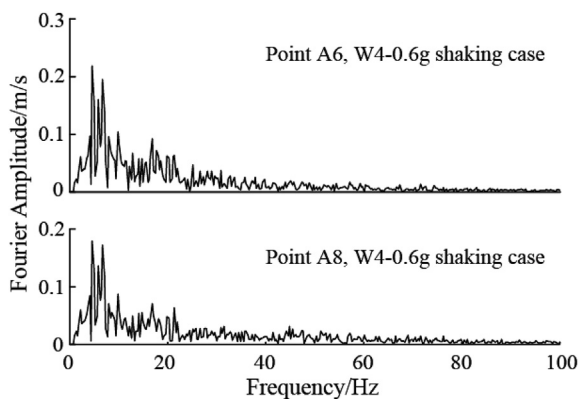


Fig. 13. Fourier spectra of backfill sands at test points A6 and A8 under W4-0.6 g shaking case.

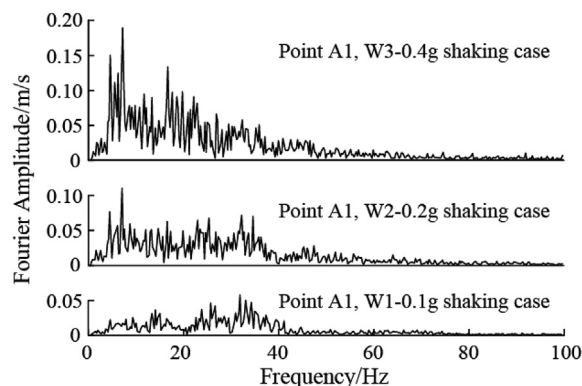


Fig. 14. Fourier spectra of the test point A1 under W1-0.1 g, W2-0.2 g and W3-0.4 g shaking cases.

earth pressure fluctuates almost synchronously with the input Wenchuan wave (cf. Fig. 8(a)). After the shaking, the baseline of the dynamic earth pressure returns to zero-line, indicating that no residual earth pressure is induced by the seismic loading.

The measured peak dynamic earth pressures (σ_H) were normalized to the soil unit weight (γ) and the wall height (H). Fig. 17 shows the distribution of the normalized peak dynamic earth pressure response behind the wall under the four shaking cases along the wall height. It demonstrates that the peak dynamic earth pressure increases with the increasing input peak acceleration at the same test point and presents

approximately a “S-shape” (i.e. “bimodal”) distribution along the wall height. Zhu et al. (2012) reported another form of the bimodal distribution for peak dynamic earth pressure response in a strip-reinforced earth retaining wall obtained by the shaking table test. The distributions have an inflection at 40 cm of height, which may due to the larger permanent lateral displacement at this height. However, as the bimodal distribution for peak dynamic earth pressure response in retaining walls has seldom been observed, further investigation and reasonable explanation are needed.

Table 2
Shaking cases of the large-scale shaking table test.

No.	Seismic wave	Shaking case	Input time (s)	Peak acceleration (g)
1	White noise	B1	30	0.05
2	Wenchuan wave	W1	32.6	0.1
3	White noise	B2	30	0.05
4	Wenchuan wave	W2	32.6	0.2
5	White noise	B3	30	0.05
6	Wenchuan wave	W3	32.6	0.4
7	White noise	B4	30	0.05
8	Wenchuan wave	W4	32.6	0.6
9	White noise	B5	30	0.05

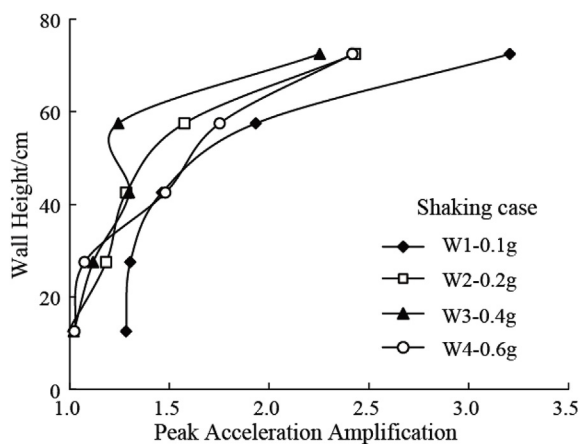


Fig. 15. Distribution of horizontal peak acceleration amplification along wall height.

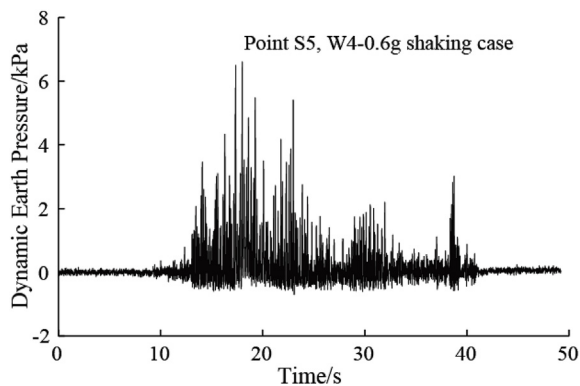


Fig. 16. Time history of dynamic earth pressure at test point S5.

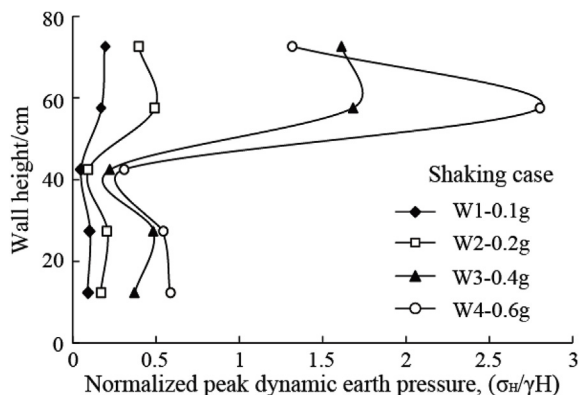


Fig. 17. Distribution of peak dynamic earth pressure coefficients along wall height.

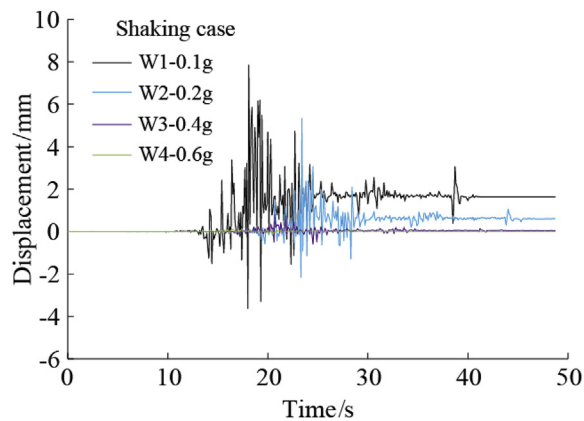


Fig. 18. Time histories of lateral displacements of wall top at test point L1.

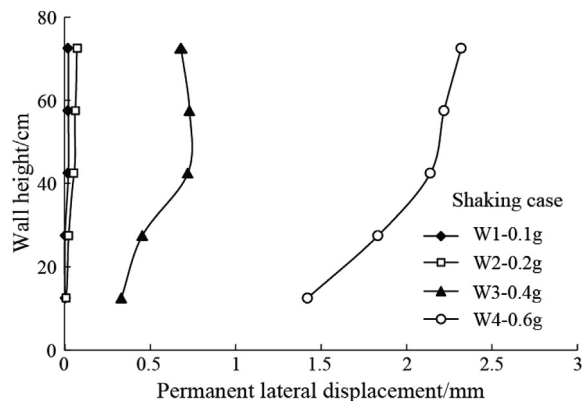


Fig. 19. Permanent lateral displacements along the wall height.

3.5.5. Lateral displacements of wall

Fig. 18 gives the time histories of lateral displacements of the wall top at test point L1 under the four shaking cases (W1-0.1 g to W4-0.6 g). It shows that the lateral displacements of the wall top are very small under the shaking cases of W1-0.1 g and W2-0.2 g, and almost no residual lateral displacements are induced. With the increase of the input peak acceleration, the lateral displacement of the wall top increases. Under the shaking case of W4-0.6 g, the peak and residual values of lateral displacement of the wall top are 7.84 mm and 1.64 mm, respectively.

Fig. 19 shows the distribution of permanent lateral displacements after four shakings along the wall height. It demonstrates that the distributions of permanent lateral displacements with small values are nearly linear along the wall height under the shaking cases of W1-0.1 g and W2-0.2 g. Under the shaking cases of W3-0.4 g and W4-0.6 g, the distributions of permanent lateral displacements are nonlinear along the wall height with a turnpoint around 45 cm wall height. The permanent lateral displacements increase significantly below the turnpoint and the increments become small above the turnpoint. After four shakings, the maximum permanent lateral displacement of the wall is 2.32 mm, 0.29% of the wall height. Usually, the lateral displacement index, defined as the ratio of the wall top displacement to the wall height, is used to evaluate the safety of retaining walls. According to the post-investigation results of the Wenchuan earthquake, if the lateral displacement index is less than 1.0%, the retaining wall could be slightly damaged. Therefore, the results of the shaking table tests indicate that the retaining wall of soilbags has a good seismic performance.

4. Conclusion

This paper presents the investigation of the seismic response of the soilbags-stacked retaining wall model through a series of small-scale shaking table tests with the input of a sinusoidal wave and different accelerations and a large-scale shaking table test in a designed laminar shear box with the input of the Wenchuan earthquake wave. The following conclusions can be obtained:

- (1) For the same size, the lateral displacement, the dynamic earth pressure and the peak acceleration amplification of the soilbags-stacked wall are less than those of the horizontally reinforced soil wall. The seismic response of the soilbags-stacked retaining wall is equivalent to or even slightly better than that of the horizontally reinforced soil wall.
- (2) The reinforcement of the top layers of soilbags can reduce significantly the lateral displacement of the wall, which provides an effective way to improve the seismic performance of the retaining wall of soilbags.
- (3) The fundamental frequencies of the retaining wall of soilbags may vary along the wall height after the shaking under the Wenchuan wave with different input peak accelerations.
- (4) Under the Wenchuan wave shaking, the peak acceleration of the retaining wall model of soilbags increases along the wall height from the bottom to the top within the frequency less than 40 Hz. Compared to the input Wenchuan wave, the Fourier amplitude of the wall model increases within the frequencies ranging from 5 to 15 Hz and is filtered out within the frequencies larger than 20 Hz. The fundamental frequency and the Fourier spectral characteristics of the soilbags' retaining wall are similar to those of backfill sands, so that the retaining wall can deform basically together with the backfill sands.
- (5) The dynamic earth pressure of the wall model fluctuates almost synchronously with the input Wenchuan wave and no residual earth pressure is induced by the seismic loading. An approximately bimodal distribution of peak dynamic earth pressure was observed along the wall height, which should be further investigated.
- (6) The permanent lateral displacements of the retaining wall model of soilbags are small when subjected to multiple shakings. The maximum ratio of the permanent lateral displacement of the wall model to the wall height is 0.29%, far less than the suggested value of 1.0% in the post-investigation of the Wenchuan earthquake. It provides a proof that the retaining wall of soilbags has a good seismic performance.

Acknowledgements

The authors greatly appreciate the support provided by National Key R&D Program of China (Grant No. 2017YFE0128900), the National Natural Science Foundation of China (Grant No. 51379066), the Fundamental Research Funds for the Central Universities (Grant No. 2018B624X14), a Project Funded by the Priority Academic Program Development of Jiangsu Higher Education Institutions (Grant No. YS11001) and Postgraduate Research & Practice Innovation Program of Jiangsu Province (Grant No. KYCX18.0593). The supports are greatly appreciated. The authors also appreciate the assessors' excellent comments and constructive suggestions to the study.

References

Bathurst, R.J., Allen, T.M., Walters, D.L., 2005. Reinforcement loads in geosynthetic walls and the case for a new working stress design method. *Geotext. Geomembranes* 23 (4), 287–322.

Bathurst, R.J., Nernheim, A., Walters, D.L., Allen, T.M., Burgess, P., Saunders, D.D., 2009. Influence of reinforcement stiffness and compaction on the performance of four geosynthetic reinforced soil walls. *Geosynth. Int.* 16 (1), 43–59.

Chen, G.X., Chen, S., Zuo, X., Du, X.L., Qi, C.Z., Wang, Z.H., 2015. Shaking-table tests and

numerical simulations on a subway structure in soft soil. *Soil Dynam. Earthq. Eng.* 76, 13–28.

Chen, G.X., Wang, Z.H., Zuo, X., Du, X.L., Han, X.J., 2010. Development of laminar shear soil container for shaking table tests. *Chin. J. Geotech. Eng.* 32 (1), 89–97 (in Chinese).

Cheng, H.Y., Yamamoto, H., Thoeni, K., 2016. Numerical study on stress states and fabric anisotropies in soilbags using the DEM. *Comput. Geotech.* 76, 170–183.

Cheng, H.Y., Yamamoto, H., Thoeni, K., Wu, Y., 2017. An analytical solution for geotextile-wrapped soil based on insights from DEM analysis. *Geotext. Geomembranes* 45 (4), 361–376.

Collin, J.G., Chouery-Curtis, V.E., Berg, R.R., 1992. Field observations of reinforced soil structures under seismic loading. In: Ochiai, H. (Ed.), *Proc., Int. Symp. on Earth Reinforcement*. Balkema, Rotterdam, The Netherlands, pp. 223–228.

Ehrlich, M., Mirmoradi, S.H., Saramago, R.P., 2012. Evaluation of the effect of compaction on the behavior of geosynthetic-reinforced soil walls. *Geotext. Geomembranes* 34, 108–115.

El-Emam, M.M., Bathurst, R.J., 2004. Experimental design, instrumentation and interpretation of reinforced soil wall response using a shaking table. *Int. J. Phys. Model. Geotech.* 4 (4), 13–32.

El-Emam, M.M., Bathurst, R.J., 2007. Influence of reinforcement parameters on the seismic response of reduced-scale reinforced soil retaining walls. *Geotext. Geomembranes* 25 (1), 33–49.

Fan, C., Liu, H., Cao, J., Ling, H.I., 2020. Responses of reinforced soil retaining walls subjected to horizontal and vertical seismic loadings. *Soil Dynam. Earthq. Eng.* 129, 105969.

Fan, K.W., Liu, S.H., Cheng, Y.P., Wang, Y., 2019. Sliding stability analysis of a retaining wall constructed by soilbags. *Geotech. Lett.* 9 (3), 211–217.

Futaki, M., Ogawa, N., Sato, M., Kumada, T., Natsume, S., 1996. Experiments about seismic performance of reinforced earth retaining wall. In: *Proc. of the 11th World Conf. on Earthquake Engineering*. Elsevier Science, New York.

Giroud, J.P., Han, J., 2004. Design method for geogrid-reinforced unpaved roads. II. Calibration and applications. *J. Geotech. Geoenviron.* 130 (8), 787–797.

Huang, C.C., Horng, J.C., Chang, W.J., Chiou, J.S., Chen, C.H., 2011. Dynamic behavior of reinforced walls e horizontal displacement response. *Geotext. Geomembranes* 29 (3), 257–267.

Huang, C.C., 2019. Seismic responses of vertical-faced wrap-around reinforced soil walls. *Geosynth. Int.* 26 (2), 146–163.

Koseki, J., 2012. Use of geosynthetics to improve seismic performance of earth structures. *Geotext. Geomembranes* 34, 51–68.

Koseki, J., Munaf, Y., Tatsuoka, F., Tateyama, M., Kojima, K., Sato, T., 1998. Shaking and tilt table tests of geosynthetic-reinforced soil and conventional-type retaining walls. *Geosynth. Int.* 5 (1–2), 73–96.

Li, L.H., Yang, J.C., Xiao, H.L., Zhang, L., Hu, Z., Liu, Y.L., 2020. Behavior of tire-geogrid-reinforced retaining wall system under dynamic vehicle load. *Int. J. GeoMech.* 20 (4), 04020017.

Lin, Y.L., Yang, G.L., Yang, X., Zhao, L.H., Shen, Q., Qiu, M.M., 2017. Response of gravity retaining wall with anchoring frame beam supporting a steep rock slope subjected to earthquake loading. *Soil Dynam. Earthq. Eng.* 92, 633–649.

Ling, H.I., Leshchinsky, D., Mohri, Y., Wang, J., 2012. Earthquake response of reinforced segmental retaining walls backfilled with substantial percentage of fines. *J. Geotech. Geoenviron. Eng.* 138 (8), 934–944.

Liu, H.B., Yang, G.Q., Ling, H.I., 2014a. Seismic response of multi-tiered reinforced soil retaining walls. *Soil Dynam. Earthq. Eng.* 61, 1–12.

Liu, H.B., Yang, G.Q., Wang, H., Xiong, B.L., 2017. A large-scale test of reinforced soil railway embankment with soilbag facing under dynamic loading. *Geomech. Eng.* 12 (4), 579–593.

Liu, S.H., 2017. *The Principle and Application of Soilbags*. Science Press, Beijing (in Chinese).

Liu, S.H., Fan, K.W., Chen, X.L., Jia, F., Mao, H.Y., Lin, Y.W., 2016. Experimental studies on interface friction characteristics of soilbags. *Chin. J. Geotech. Eng.* 38 (10), 1874–1880 (in Chinese).

Liu, S.H., Fan, K.W., Xu, S.Y., 2019. Field study of a retaining wall constructed with clay-filled soilbags. *Geotext. Geomembranes* 47 (1), 87–94.

Liu, S.H., Gao, J.J., Wang, Y.Q., Weng, L.P., 2014b. Experimental study on vibration reduction by using soilbags. *Geotext. Geomembranes* 42 (1), 52–62.

Liu, S.H., Jia, F., Shen, C.M., Weng, L.P., 2018. Strength characteristics of soilbags under inclined loads. *Geotext. Geomembranes* 46 (1), 1–10.

Liu, S., Lu, Y., Weng, L., Bai, F., 2015. Field study of treatment for expansive soil/rock channel slope with soilbags. *Geotext. Geomembranes* 43 (4), 283–292.

Liu, S.H., Xue, X.H., Fan, K.W., Xu, S.Y., 2014c. Earth pressure and deformation mode of a retaining wall constructed with soilbags. *Chin. J. Geotech. Eng.* 36 (12), 2267–2273 (in Chinese).

Matsuoka, H., Chen, Y., Kodama, H., Yamaji, Y., Tanaka, R., 2000a. Mechanical properties of soilbags and unconfined compression tests on model and real soilbags. *Proc. of the 35th Japan National Conf. on Geotechnical Engineering*. 544, 1075–1076 (in Japanese).

Matsuoka, H., Liu, S.H., 1999. Bearing capacity improvement by wrapping a part of foundation. 617/III-46. *Jpn. Soc. Civ. Eng. (JSCE)* 235–249 (in Japanese).

Matsuoka, H., Liu, S.H., 2003. New earth reinforcement method by soilbags (“Donow”). *Soils Found.* 43 (6), 173–188.

Matsuoka, H., Liu, S.H., 2006. *A New Earth Reinforcement Method Using Soilbags*. Taylor & Francis/Balkema, the Netherlands.

Matsuoka, H., Yamaguchi, K., Liu, S.H., Kodama, H., Yamaji, Y., 2000b. Construction cases of retaining walls and building foundation improvement by soilbags. In: *Proc. of the 35th Japan National Conf. on Geotechnical Engineering*. 545. pp. 1077–1078 (in Japanese).

- Moghaddas Tafreshi, S.N., Khalaj, O., Dawson, A.R., 2014. Repeated loading of soil containing granulated rubber and multiple geocell layers. *Geotext. Geomembranes* 42 (1), 25–38.
- Nakajima, S., 2008. Study on seismic performance of geogrid reinforced soil retaining walls and deformation characteristics of backfill soil. In: 4th Asian Regional Conf. on Geosynthetics, Shanghai, China.
- Plácido, R., Portelinha, F.H.M., Futai, M.M., 2018. Field and laboratory time-dependent behaviors of geotextiles in reinforced soil walls. *Geosynth. Int.* 25 (2), 215–229.
- Ren, F., Huang, Q., Wang, G., 2020. Shaking table tests on reinforced soil retaining walls subjected to the combined effects of rainfall and earthquakes. *Eng. Geol.* 105475.
- Riccio, M., Ehrlich, M., Dias, D., 2014. Field monitoring and analyses of the response of a block-faced geogrid wall using fine-grained tropical soils. *Geotext. Geomembranes* 42 (2), 127–138.
- Rowe, R.K., Skinner, G.D., 2001. Numerical analysis of geosynthetic reinforced retaining wall constructed on a layered soil foundation. *Geotext. Geomembranes* 19 (7), 387–412.
- Sabermahani, M., Ghalandarzadeh, A., Fakher, A., 2009. Experimental study on seismic deformation modes of reinforced-soil walls. *Geotext. Geomembranes* 27 (2), 121–136.
- Skinner, G.D., Rowe, R.K., 2005. Design and behavior of a geosynthetic reinforced retaining wall and bridge abutment on a yielding foundation. *Geotext. Geomembranes* 23 (3), 234–260.
- Sukmak, K., Han, J., Sukmak, P., Horpibulsuk, S., 2016. Numerical parametric study on behavior of bearing reinforcement earth walls with different backfill material properties. *Geosynth. Int.* 23 (6), 435–451.
- Tatsuoka, F., Tateyama, M., Koseki, J., 1996. Performance of soil retaining walls for railway embankments. *Soils Found.* 36 (S), 311–324.
- Tavakoli Mehrjardi, G.H., Moghaddas Tafreshi, S.N., Dawson, A.R., 2012. Combined use of geocell reinforcement and rubber-soil mixtures to improve performance of buried pipes. *Geotext. Geomembranes* 34 (1), 116–130.
- Wang, L., Liu, H., Wang, C., 2018. Earth pressure coefficients for reinforcement loads of vertical geosynthetic-reinforced soil retaining walls under working stress conditions. *Geotext. Geomembranes* 46 (4), 486–496.
- Wang, L.J., Liu, S.H., Liao, J., Fan, K.W., 2019a. Field load tests and modelling of soft foundation reinforced by soilbags. *Geosynth. Int.* 26 (6), 580–591.
- Wang, L.J., Liu, S.H., Zhou, B., 2015a. Experimental study on the inclusion of soilbags in retaining walls constructed in expansive soils. *Geotext. Geomembranes* 43 (1), 89–96.
- Wang, L.Y., Chen, G.X., Chen, S., 2015b. Experimental study on seismic response of geogrid reinforced rigid retaining walls with saturated backfill sand. *Geotext. Geomembranes* 43 (1), 35–45.
- Wang, Y.Q., Li, X., Liu, K., Liu, G., 2019b. Experiments and DEM analysis on vibration reduction of soilbags. *Geosynth. Int.* 26 (5), 551–562.
- Wang, Y.Q., Liu, K., Li, X., Ren, Q.B., Li, L.L., Zhang, Z.H., Li, M.C., 2019c. Experimental and upper-bound study of the influence of soilbag tail length on the reinforcement effect in soil slopes. *Geotext. Geomembranes* 47 (5), 610–617.
- Yang, G.Q., Liu, H.B., Lv, P., Zhang, B.J., 2012. Geogrid-reinforced lime-treated cohesive soil retaining wall: case study and implications. *Geotext. Geomembranes* 35, 112–118.
- Yazdandoust, M., 2017a. Investigation on the seismic performance of steel-strip reinforced-soil retaining walls using shaking table test. *Soil Dynam. Earthq. Eng.* 97, 216–232.
- Yazdandoust, M., 2017b. Experimental study on seismic response of soil-nailed walls with permanent facing. *Soil Dynam. Earthq. Eng.* 98, 101–119.
- Yazdandoust, M., 2018. Seismic performance of soil-nailed walls using a 1 g shaking table. *Can. Geotech. J.* 55 (1), 1–18.
- Yu, Y., Bathurst, R.J., Allen, T.M., 2017. Numerical modelling of two full-scale reinforced soil wrapped-face walls. *Geotext. Geomembranes* 45 (4), 237–249.
- Zhang, J., Qu, H.L., Liao, Y., Ma, Y.X., 2012. Seismic damage of earth structures of road engineering in the 2008 Wenchuan earthquake. *Environ. Earth Sci.* 65 (4), 987–993.
- Zhu, H.W., Yao, L.K., Liu, Z.S., 2012. Comparison of dynamic characteristics between netted and packaged reinforced soil retaining walls and recommendations for seismic design. *Chin. J. Geotech. Eng.* 34 (11), 2072–2080 (in Chinese).